Electronic properties of the interface between *p*-CuI and anatase-phase *n*-TiO_2 single crystal and nanoparticulate surfaces: A photoemission study

A. R. Kumarasinghe, W. R. Flavell,[a] A. G. Thomas, A. K. Mallick, D. Tsoutsou, C. Chatwin, S. Rayner, P. Kirkham, and S. Warren[b]
School of Physics and Astronomy, The University of Manchester, Sackville Street Building, P.O. Box 88, Manchester M60 1QD, United Kingdom

S. Patel
CCLRC Daresbury Laboratory, Warrington, Cheshire WA4 5AD, United Kingdom

P. Christian and P. O'Brien
School of Chemistry, The University of Manchester, Oxford Road, Manchester M13 9PL, United Kingdom

M. Grätzel and R. Hengerer
Swiss Federal Institute of Technology, Laboratory for Photonics and Interfaces, Chemin des Alambics, CH-1015 Lausanne, Switzerland

(Received 9 March 2007; accepted 21 July 2007; published online 18 September 2007)

We present a study of the growth of the *p*-type inorganic semiconductor CuI on *n*-type TiO_2 anatase single crystal (101) surfaces and on nanoparticulate anatase surfaces using synchrotron radiation photoemission spectroscopy. Core level photoemission data obtained using synchrotron radiation reveal that both the substrate (TiO_2) and the overlayer (CuI) core levels shift to a lower binding energy to different degrees following the growth of CuI on TiO_2. Valence band photoemission data show that the valence band maximum of the clean substrate differs from that of the dosed surface which may be interpreted qualitatively as due to the introduction of a new density of states within the band gap of TiO_2 as a result of the growth of CuI. The valence band offset for the heterojunction *n*-TiO_2/*p*-CuI has been measured using photoemission for both nanoparticulate and single crystal TiO_2 surfaces, and the band energy alignment for these heterojunction interfaces is presented. With the information obtained here, it is suggested that the interface between *p*-CuI and single crystal anatase-phase *n*-TiO_2 is a type-II heterojunction interface, with significant band bending. The measured total band bending matches the work function change at the interface, i.e., there is no interface dipole. In the case of the nanoparticulate interface, an interface dipole is found, but band bending within the anatase nanoparticles remains quite significant. We show that the corresponding depletion layer may be accommodated within the dimension of the nanoparticles. The results are discussed in the context of the functional properties of dye-sensitized solid state solar cells. © *2007 American Institute of Physics*. [DOI: 10.1063/1.2772249]

I. INTRODUCTION

Semiconductor heterojunction interfaces exhibit interesting and useful electronic properties associated with the discontinuity in the local band structure at the interface. As a result, such heterostructures have become important as a basis for novel devices. One example of such devices is the solid state dye-sensitized solar cell, which offers a potentially cost-effective and easy to manufacture light-to-electrical energy conversion system.[1–7] In the most efficient dye-sensitized solar cell,[1,2] a porous nanocrystalline TiO_2 film stained by a ruthenium bipyridyl-based dye is used in contact with a liquid electrolyte, and the key processes take place at the interface between the dye-sensitized nanostructured film and the liquid electrolyte. The liquid electrolyte may degrade over a period of time due to problems such as seal imperfections or vaporization. These problems have encouraged the search for suitable solid materials that can replace the liquid electrolyte. In such solid state solar cells, the solid hole-conducting material captures the positive charges from the oxidized dye that are left behind as a result of optical excitation. Hole conductors so far considered include polymer-gel electrolytes,[8] conducting organic polymers,[9] ionic conductive polymer electrolytes,[10] organic hole conductors,[11] and inorganic semiconductors such as CuI and CuCNS.[12,13] Among these materials, CuI (copper (I) iodide) has shown promising results when employed as a hole-conducting material in dye-sensitized solar cells (Ref. 14 and reference therein). Copper (I) iodide is a *p*-type semiconductor with a band gap of ~3.1 eV,[15,16] which can be deposited from a solution of acetonitrile onto dye-sensitized substrates using a low temperature deposition technique. The use of low temperature to deposit CuI on TiO_2 has the advantage that CuI can be grown on dye-sensitized surfaces without denaturing the dye monolayer. This is very important as this may influence the light absorption properties of the dye and

[a]Author to whom correspondence should be addressed. Tel.: 0044-161-306-4466; Electronic mail: wendy.flavell@manchester.ac.uk
[b]Present address: CCLC Nantes Atlantique, Centre René Gauducheau, Blvd. Prof. Jacques Monod, 44805 St. Herblain, France.

hence the overall function of the cell. Furthermore CuI can also be deposited as a transparent thin film on conducting glass substrates under suitable conditions and (in the case of our experiments) is readily deposited in vacuum by evaporation.

The photoconversion yield of dye-sensitized solid state heterojunction solar cells largely depends on the charge transfer processes at the interface, which in turn depend on the energy level matching of the dye and the two semiconducting materials used. The band offset at the heterojunction interface is one of the most important properties of the junction and can be used to design and optimize the cell characteristics.[17] Photoemission spectroscopy is a powerful tool to investigate band offsets at semiconductor heterojunctions. Photoemission has successfully been used in the recent past to investigate electronic properties at the interfaces between organic/inorganic[18–21] and inorganic/inorganic[17,22–25] systems with high precision. The information obtained from core level binding energy shifts and valence band photoemission spectra can be used to investigate any possible band-bending effects at the interface and also to determine the band energy offset and energy level matching at the interface.

We have previously studied the adsorption of bi-isonicotinic acid (part of the ligand structure of the Ru bipyridyl dye) on anatase TiO_2 (101) and (001) using photoemission and near-edge x-ray absorption fine structure.[26] The interaction between a Ru (II) dye molecule and both nanoparticulate anatase and CuI at the TiO_2/CuI interface has been studied by Karlsson *et al.*[27] In the present study we focus our attention on model "dye-free" interfaces fabricated by the deposition of CuI onto the surfaces of single crystal anatase TiO_2 (101) and nanoparticulate thin films of TiO_2 in ultrahigh vacuum (UHV), in order to model the heterojunction at the heart of the *p*-CuI/*n*-TiO_2 solid state solar cell. The electronic structure at the interface between bulk anatase single crystal and CuI is compared with that between nanoparticulate anatase thin films and CuI. It is possible to estimate the band energy lineup at this interface using flatband potential measurements of the individual materials. However, this neglects any possible band bending effects and dipole effects at the interface. These are investigated here. In the liquid-phase devices, band-bending is thought not to occur, as the TiO_2 nanoparticles are assumed to be too small to maintain the necessary depletion layer, and they are in any case screened by the surrounding electrolyte.[2] The solid state junctions are less well studied and the heterojunction between the *p*- and *n*-type materials might be expected to show band-bending effects. To the best of our knowledge, there are no previous reports of direct experimental determination of band offsets in the CuI/TiO_2 system. In principle, accurate determination of the energy level lineup at this heterojunction could help guide the choice of sensitizing dye for optimum interface charge transfer.

II. EXPERIMENT

The photoemission experiments were carried out on the multipole wiggler beamline MPW6.1 (PHOENIX, photon energy range of $30 \leqslant h\nu \leqslant 350$ eV) at the CCLRC Daresbury Laboratory. Core level and valence band photoemission spectra were recorded with the samples at an angle of 45° to the incident photons and close to normal emission. All spectra were recorded with the sample at room temperature and are referenced to a Fermi edge recorded from a sputtered Ta clip holding the sample in place and normalized to the I_0 (flux) monitor of the beamline. I_0 was recorded using a W mesh placed in the beamline just prior to the point where light enters the experimental chamber. The total (analyzer + monochromator) resolution was 140 meV for the valence band scans. The base pressure in the chamber was around 5×10^{-10} mbar during the experiments.

TiO_2 anatase crystals [with 2×4 mm^2 (101) surfaces] were grown by a chemical transport method.[28] The samples were deep red when supplied. Prior to the supply, the crystals were characterized by low energy electron diffraction (LEED) and secondary electron diffraction.[29] Prior to the photoemission experiments, the orientation of the surface under investigation was confirmed by Laue back reflection aided by simulations of the Laue pattern using Lauegen software.[30] The anatase TiO_2 single crystal was mounted onto a Ta sample plate using Ta clips, on a UHV sample manipulator. The experimental chamber was equipped with an ARUPS10 multichannel hemispherical analyzer, electron gun, LEED apparatus, and Ar^+-ion etcher. Clean, ordered surfaces were prepared by repeated cycles of Ar^+-ion sputtering (1.0 keV) and annealing to 700 °C (by electron bombardment of the back of the sample plate) until the surface was free from C and other contaminants. Ar^+ ion etching is well known to create surface oxygen vacancies and associated electron carriers at TiO_2 surfaces,[31] so the single crystal surfaces produced are nonstoichiometric. The sample temperature was measured using an optical pyrometer. Annealing was carefully controlled to ensure no phase transition occurred during annealing. This treatment resulted in a sharp (1×1) LEED pattern for the (101) surface, in agreement with previous LEED measurements for this surface.[29] Following this preparation, no further change in the defect concentration (as gauged by the intensity of the so-called defect peak observed at around 1 eV binding energy[31]) was observed as a function of time in UHV.

Nanoparticulate thin films of anatase-phase TiO_2 were prepared by a sol-gel route involving the hydrolysis of $TiCl_4$ in hexdecylamine at 180 °C, followed by dissolution in toluene and precipitation with isopropanol. The precipitated material was deposited using a doctor blade technique on F-doped SnO_2 substrates (Solaronix, $\sim 17\ \Omega\ \mathrm{cm}^{-2}$), and annealed for 2 h at 450 °C.[32] Transmission electron microscopy measurements revealed a narrow particle-size distribution with an average particle size of 7.3 ± 1 nm, while x-ray diffraction showed only the presence of anatase-phase TiO_2.[32] For photoemission experiments, the TiO_2 nanoparticle film electrodes were glued onto stainless steel sample holders using UHV-compatible Ag-based conducting glue. To prevent possible surface charging effects during the photoemission experiments, it was necessary to ensure a good electrical contact between the substrate and the stainless steel sample holder. This was achieved by making a conducting

bridge between those two surfaces using the Ag-based glue. In order not to sinter the films, destroying their nanoparticulate structure, the films were studied in the as-presented state, without annealing, etching, or any other surface treatment. No change in the oxygen content of the surface was observed as a function of time in UHV.

CuI dosing was carried out on the anatase TiO_2 (101) surface and the nanoparticulate TiO_2 thin films in UHV from a well outgassed powder source using a homebuilt Knudsen-type cell. Outgassing of the CuI powder (Aldrich 99.99%) was carried out by repeated heating to a temperature of 185–235 °C in a separate vacuum chamber which was isolated from the main chamber. During dosing, the getter source was held at a temperature of ~205 °C with the sample held at room temperature and approximately 1 cm away from the getter source. A thermocouple attached close to the nozzle of the Knudsen-type cell was used to measure the dosing temperature. By varying the length of the time of the dosing, the thickness of CuI layer on TiO_2 was varied. Dosing was carried out after a constant evaporation rate was achieved, as monitored by the chamber pressure. After each growth step, photoelectron spectra were taken from the valence band and Ti 3*p*, Cu 3*p*, and I 4*d* core levels. Auger electron spectroscopy (AES) was used as a secondary characterization. Secondary electron energy distribution (SEED) curves were taken after each growth of CuI with a sample bias of −37.9 V in order to determine the work function of the sample. The negative sample bias enabled the evolution of the SEED edge to be monitored clearly.

Core level photoemission and AES were used to determine the stoichiometry of the deposited films. In some cases, following very long deposition times, the stoichiometry of the film was found to depart from the expected 1:1 ratio in CuI, and widely varying stoichiometries including Cu_4I, CuI_2, and CuI_3 were observed. Here, we present only data from deposited films where the stoichiometry was found to be CuI within experimental error. No evidence was found in AES or core level photoemission for formation of CuO or any other Cu (II) species. For stoichiometric films, core level photoemission and AES data were used to determine an approximate film thickness, assuming that the CuI film was deposited as a uniform overlayer.[33] This is clearly an approximation, as CuI is believed to be deposited onto nanoparticulate TiO_2 as clusters; layer-by-layer growth is not observed.[27]

III. RESULTS AND DISCUSSION

A. The anatase single crystal (101)/CuI interface

Figure 1(a) shows core level photoemission spectra of the Ti 3*p* signal for the anatase TiO_2 (101) surface as the surface is dosed with CuI. In common with all the core level and valence band spectra presented here, a fourth order polynomial background has been subtracted, and the spectra are aligned on a binding energy scale relative to a Fermi edge recorded from a Ta clip in contact with the sample. Unless stated, all spectra have been normalized to the incident photon flux. Starting with the clean surface data, the Ti 3*p* spectrum shows a peak at a binding energy of 37.8±0.1 eV. The spectral line shape and the peak position of the Ti 3*p* core level for the clean surface are in good agreement with earlier studies of the anatase (101) surface, and have been discussed previously.[26] Upon CuI dosing, the intensity of the Ti 3*p* peak is attenuated, while the peak position is shifted to a lower binding energy (BE). After a total of 30 min dose, the peak maximum lies at a binding energy of 37.3±0.1 eV, a shift to lower BE of 0.5±0.1 eV. This pronounced shift in BE of the substrate core level following the dose of CuI indicates the formation of a space-charge-like layer (band bending) in the substrate.[17] Core level photoemission spectra can also distinguish the bonding environment of surface and near-surface atoms and changes induced by the adsorption of molecules on the surface. The formation of covalent or ionic bonds should result in chemically shifted components.[18] There are no significant changes in spectral line shape of the substrate core level features following CuI dosing which implies that strong chemical bonds are not formed between TiO_2 and CuI. This suggests that the interaction between TiO_2 and CuI is weak and the interface is abrupt.

Turning to the I 4*d* and the Cu 3*p* core level photoemission spectra shown in Figs. 1(b) and 1(c), we observe an increase in the intensity of both core level signals with dosing. Both I 4*d* and Cu 3*p* signals shift to lower BE with increasing levels of CuI dosing. The BE shift for the Cu 3*p* core level is 0.3±0.1 eV after a total of 30 min dose. The BE shift for the I 4*d* peaks is 0.2±0.1 eV for the same dosing time. The magnitude of the shift of the Cu core level to lower BE on CuI dosing is consistent with a previous study,[27] although the expected corresponding shift of the I core levels was not observed previously.[27] The disagreement in BE shifts observed for the I core levels may lie in the nature of the two interfaces under investigation, as a monolayer of dye molecules was also present on the surface of TiO_2 in the work reported in Ref. 27. As was observed for the Ti 3*p* core level spectra, the spectral line shape and width of the I 4*d* core levels are not affected by increasing the level of dosing. For the Cu 3*p* level, a small increase in full width at half maximum (FWHM) of the peak of the order of 0.1 eV is observed on increasing the dosing level, perhaps suggesting that there may be a slight increase in roughness of the deposited overlayer with deposition time.[27] However, this increase is not significant compared with the experimental error. Overall, the data reinforce the idea that the interface between the single crystal TiO_2 (101) and CuI is abrupt and no significant chemical reaction takes place following the deposition process.

Figure 2 shows the evolution of the SEED edge for the clean and CuI-dosed anatase TiO_2 (101) surface. The spectra were recorded with a negative sample bias of −37.9 V. The SEED edge energy position provides useful information to calculate the work function ϕ of the sample, as when corrected for bias, it corresponds to the zero of electron kinetic energy. The work function is thus obtained by subtracting the photon energy from the bias-corrected binding energy position of the SEED edge. The SEED edge was determined here as the point where two extrapolated edges, one describing the background and the other describing the rising edge of

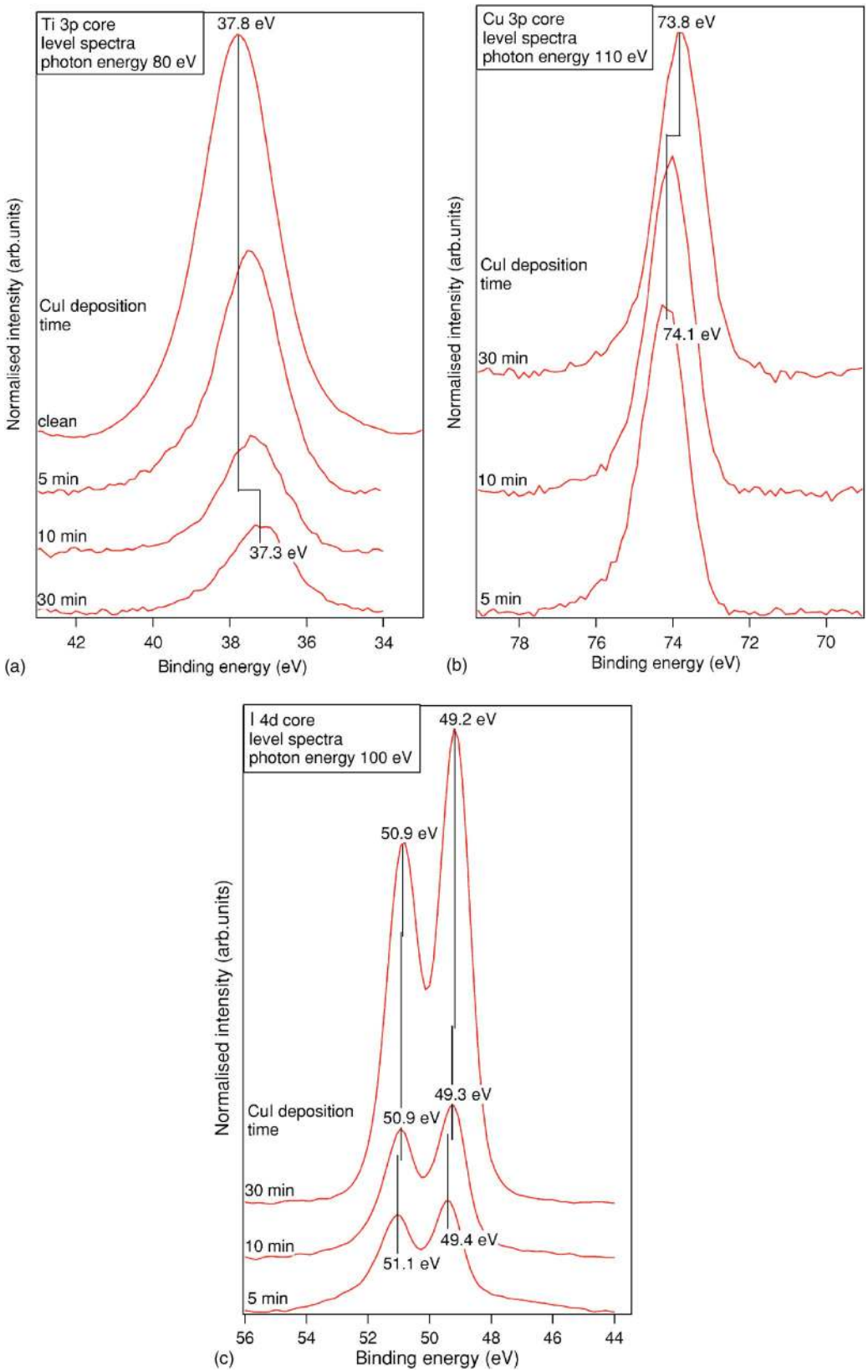

FIG. 1. Core level spectra for the clean and CuI-dosed anatase TiO_2 (101) surface at different dosing intervals. (a) Ti 3*p* core level spectra; (b) Cu 3*p* core level spectra; and (c) I 4*d* core level spectra.

the spectrum in the low kinetic energy region, intercept each other.[34] The method used for determination of the SEED edge is shown in Fig. 2. The SEED edge for the clean TiO_2 anatase (101) surface shifts to a lower BE by ~0.7±0.1 eV following dosing with CuI for 30 min. The value of the work function extracted for the clean TiO_2 anatase (101) surface is 4.7±0.1 eV.

Figure 3 shows the valence band photoemission spectra

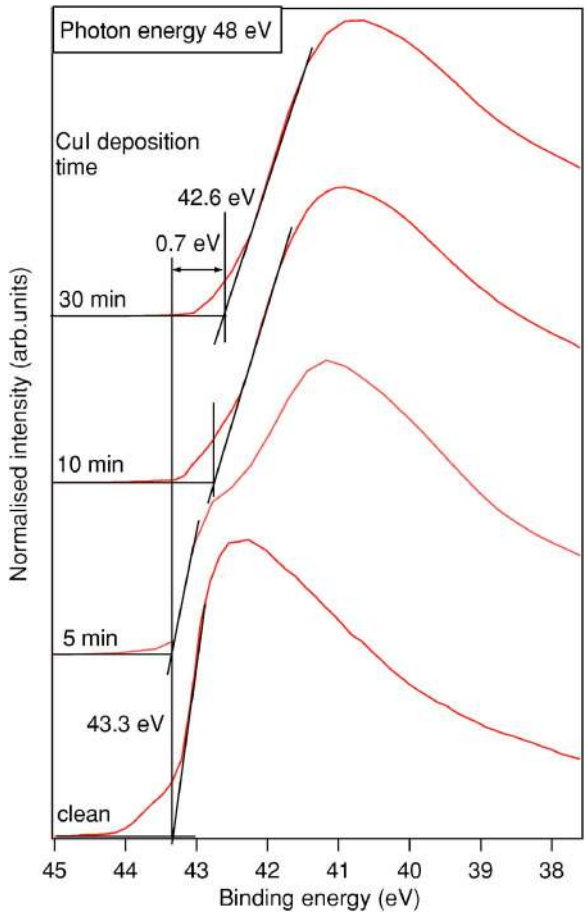

FIG. 2. Secondary electron energy distribution (SEED) spectra recorded from the anatase TiO_2 (101) surface before and after CuI dosing. CuI dosing intervals are the same as in Figs. 1(a)–1(c). The spectra were recorded while applying a negative bias of −37.9 eV to the sample; this has been accounted for in aligning the spectra on a binding energy scale. The method used to determine the SEED edge position is described in the text and is shown in the figure (Ref. 34).

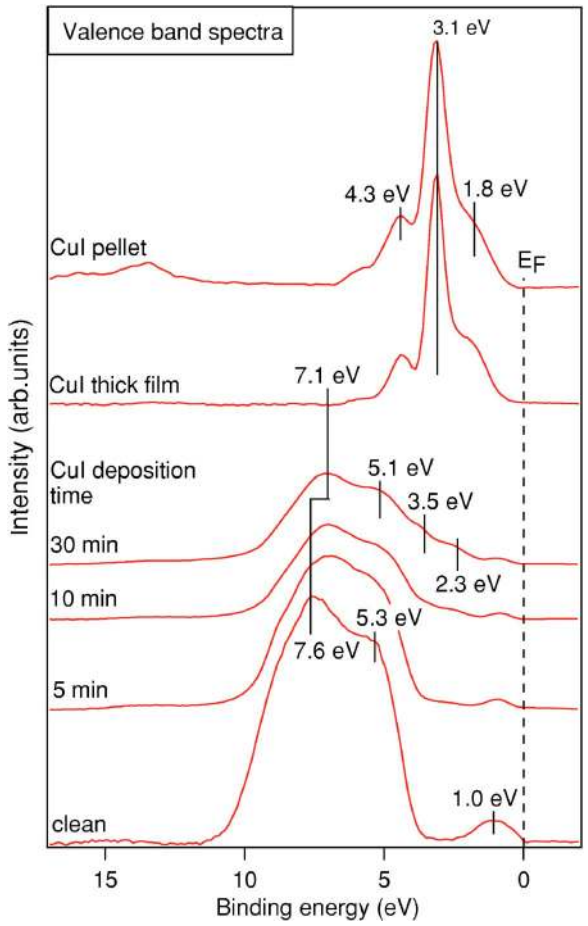

FIG. 3. Valence band energy distribution curves (EDCs) of the anatase TiO_2 (101) surface before and after CuI dosing at different dosing intervals. For low coverages (dosing intervals of 0–30 min), the spectra are normalized to the incident photon flux and are taken at the same dosing intervals as in Figs. 1(a)–1(c). For comparison, valence band EDCs recorded from a thick film of CuI (>40 Å thick) deposited on the anatase TiO_2 (101) surface and a CuI pellet are also shown in the same figure. Spectra were recorded at 47 eV photon energy for the clean and CuI-dosed anatase TiO_2 (101) surfaces. For the CuI pellet, the spectrum was recorded at 70 eV photon energy.

of the TiO_2 (101) surface before and after the growth of CuI at different dosing intervals. We have discussed the valence band electronic structure of the anatase TiO_2 (101) and (001) surfaces in detail elsewhere.[31] Here, we focus on a discussion of the effect of CuI dosing on certain features in the valence band spectra of the clean surface and on the new density of states that is introduced on dosing. In general, the valence band spectrum for the clean TiO_2 (101) surface observed in this work is in good agreement with our previous work[31] and also is in agreement with valence band spectra recorded from natural anatase crystals using an x-ray source.[35]

For the clean anatase (101) surface, there are three major peaks lying at BEs of around 7.6±0.1, 5.3±0.1, and 1.0±0.1 eV. The first two of these make up the valence band, which is around 6 eV wide and is expected to be derived mainly from O 2*p* states as in the case of rutile TiO_2.[36] The states to low binding energy (giving rise to the feature at 5.3 eV BE) have been assigned mainly to Ti 3*d*-O 2*p* π-bonding states, while at higher binding energy (the feature at 7.6 eV BE), states arising predominantly from O 2*p*-Ti 3*d* σ bonding are found.[31,35–37] The peak at a BE of 1.0±0.1 eV is derived from Ti 3*d* states which originate as a result of surface oxygen vacancies resulting in the formation of $Ti^{3+}(d^1)$. Upon CuI dosing for 30 min, the feature at a BE of 7.6±0.1 eV in the valence band of TiO_2 shifts to a lower BE by 0.5±0.1 eV. This shift is similar to that observed for the Ti 3*p* core level at the same dosing level [Fig. 1(a)]. In addition, the valence band is broadened at its lower BE side with the introduction of new features within the band gap region. The intensity of the TiO_2 valence band features diminishes gradually with increasing dosing level, suggesting that an overlayer is progressively grown on the surface of the TiO_2. After a total of 30 min dose, the features of the substrate remain dominant. If the dosing time is increased further, it is possible to produce a surface where features which can be ascribed to CuI dominate the spectrum, as shown in Fig. 3 and discussed in more detail below. In photoemission studies of other heterojunction systems, it has been observed that when the system reaches a stage in the deposition process where the valence band spectra show both the substrate and the adsorbate emissions, the thickness of the deposited layer typically lies in the range of 5–30 Å.[38] The thickness of the deposited CuI layer on TiO_2 can be estimated by the

method outlined in Sec. II, in which we assume the CuI forms a homogeneous overlayer. This yields an estimate of the thickness of the overlayer after 30 min deposition of 4 ± 1 Å. The ambient temperature γ phase of CuI has the zinc blende structure with a cubic unit cell containing four molecules per cell and unit cell parameter of 6.05 Å.[39] Thus the overlayer deposited corresponds to less than 1 unit cell thickness (and slightly more than one CuI layer). As a recent photoemission study of CuI adsorbed on nanoparticulate TiO_2 suggests that this method of CuI deposition leads to the formation of CuI clusters rather than a layer-by-layer growth,[27] we assume that the overlayer may not uniformly cover the surface. Indeed, it was possible at dosing times of up to 30 min to observe an undistorted substrate (1×1) LEED pattern after each deposition of CuI onto the TiO_2 (101) surface, with the intensity of the pattern decreasing with increasing dosing time. This pattern could not be observed for very high dosing times (where the photoemission spectrum was dominated by the features of CuI). This suggests that the TiO_2 surface is not uniformly covered by CuI after 30 min dosing, even though the amount of material deposited approximates to a coverage of more than a single monolayer of CuI.

The observation of features within the band gap of TiO_2 (i.e., above the valence band maximum and below Fermi edge) following the deposition of CuI confirms that the valence band maximum of CuI lies above that of TiO_2. This is of course a prerequisite for the hole conductor in a solid state solar cell device, as otherwise efficient electron-hole-pair separation cannot be achieved. The new features in the valence band introduced as a result of CuI dosing lie at BEs of 3.5 ± 0.1 and 2.3 ± 0.1 eV. These features grow progressively with increasing dosing time. At long dosing times, the spectrum becomes dominated by features which can be assigned to CuI, as shown in Fig. 3, where spectra recorded from both a thick deposited film (of estimated thickness >40 Å) and a polycrystalline CuI pellet are given for comparison. The valence band electronic structure of CuI thin films and CuI pellets[33,40–42] has been studied using photoemission and resonant photoemission studies. Based on these studies, assignment of the features seen in the dosed spectra of Fig. 3 is now possible. The valence band of CuI is characterized by three main features.[33,41,42] The feature lying at a BE of 3.5 ± 0.1 eV in Fig. 3 has Cu $3d$ atomic character.[42] For bulk CuI samples, it lies at a BE of 3.1 ± 0.1 eV,[33] as shown in Fig. 3. The feature at a BE of 2.3 ± 0.1 eV seen on the dosed surfaces in Fig. 3 is associated with states formed by hybridization of Cu $3d$ and I $5p$ orbitals. This feature occurs at a BE of 1.8 ± 0.1 eV for bulk samples (Fig. 3). The valence band of CuI contains a further peak lying at a BE of 4.3 ± 0.1 eV which is thought to originate from states having predominantly I $5p$ orbital character.[41,42] At low dosing levels, this state is masked by the stronger valence band features of TiO_2 at around 5 eV BE. At the interface, it is clear that the valence band features of CuI are shifted and appear at higher BE values compared to those in the bulk state of the CuI pellet or a thick film of CuI (Fig. 3). Conversely, the features remaining due to the TiO_2 valence band are shifted to lower BE compared with the undosed TiO_2 surface (for example, the strongest valence band feature of the undosed surface at 7.6 ± 0.1 eV BE is shifted to 7.1 ± 0.1 eV BE after 30 min dosing, as shown in Fig. 3). These shifts are consistent with the downward band bending that we anticipate at the surface of the p-type material and the upward band bending that we expect at the surface of the n-type material at a p-n junction. The energy level alignment at the interface is discussed in the next section.

B. Energy level alignment at the anatase TiO_2(101)/CuI interface

Photoemission spectra from a heterojunction interface may be used to extract the band energy profile at the interface. The valence band offsets at the interface (which are themselves functions of the coverage) are determined from the relative BE positions of the core level features of the heterojunction with respect to the valence band maximum (VBM).[17,22–25] The core level binding energies are typically extracted from spectra taken at coverages where both the substrate and the overlayer emission are present.[22] The valence band offset $\Delta E_V^{s/f}$ is given by[22]

$$\Delta E_V^{s/f}(\Theta) = \Delta \mathrm{BE}_{\mathrm{CL}}^{s/f}(\Theta) + (\mathrm{BE}_{\mathrm{CL}}^{s} - \mathrm{BE}_{\mathrm{VBM}}^{s}) - (\mathrm{BE}_{\mathrm{CL}}^{f} - \mathrm{BE}_{\mathrm{VBM}}^{f}), \quad (1)$$

where s and f denote substrate and overlayer film, respectively, CL refers to a core level signal and VBM to the valence band maximum. $\Delta BE_{\mathrm{CL}}^{s/f}(\Theta)$ is the binding energy difference of (chemically) unchanged core or valence band emissions of the substrate (s)/overlayer film (f) at a given coverage Θ. If the values of the band gap energies (E_{BG}) are known, the conduction band offset at the interface can also be calculated and is given by

$$\Delta E_C^{s/f} = \Delta E_V^{s/f} - (E_{\mathrm{BC}}^{f} - E_{\mathrm{BC}}^{s}). \quad (2)$$

This procedure requires a knowledge of the position of the VBM for the substrate and the overlayer. These are generally determined from a bulk standard of the substrate and an overlayer thick film, respectively.

Figures 4(a) and 4(b) show the method used to determine the VBMs of the anatase TiO_2 single crystal (101) surface and of CuI. For this purpose, a clean anatase TiO_2 (101) surface and a thick film of CuI (estimated via the approaches described earlier to be >40 Å thick) deposited on the anatase TiO_2 single crystal (101) surface were chosen. The VBM energy position is determined here from the intercept of two linear extrapolations, one describing the background and the other describing a tangent drawn at the inflection point of the spectrum at the low binding energy side of the valence band. This procedure has been used successfully for the determination of VBMs for semiconductor heterojunction interfaces[34] and in the present case yields convincing values for the VBMs of the TiO_2/CuI system. By following the procedure described above, a value of 2.9 ± 0.1 eV was obtained as the VBM energy position for the anatase TiO_2 single crystal (101) surface, while a value of 0.5 ± 0.1 eV was obtained for CuI. Given that anatase TiO_2 has a bulk band gap of ~3.2 eV[28] and is a n-type material, where the Fermi level is expected to be pinned slightly below the conduction

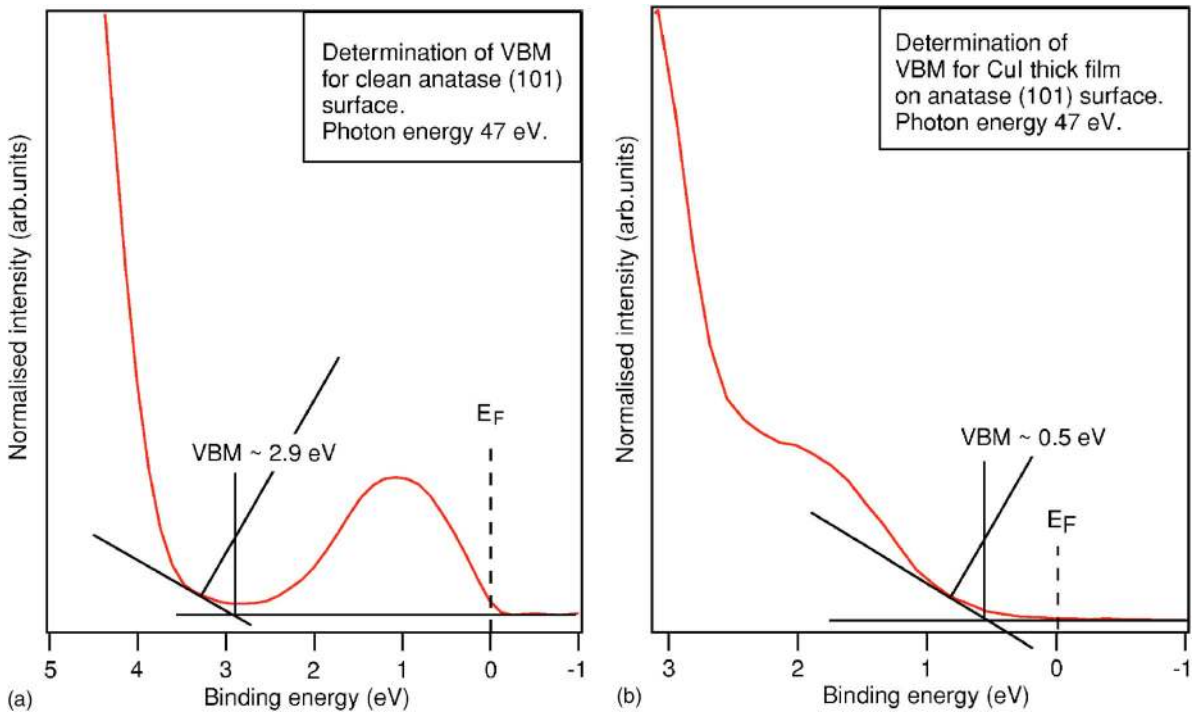

FIG. 4. Determination of the valence band maximum (VBM) for the clean anatase TiO_2 (101) surface and for CuI. VBM is taken as the point where two extrapolated edges, one describing the background and the other describing a tangent drawn at the inflection point at the low binding energy region of the spectrum, intercept each other (Ref. 34). (a) VBM determination for the clean anatase TiO_2 (101) surface and (b) VBM determination for CuI, using a spectrum recorded from a thick film (>40 Å thick) of CuI deposited on anatase TiO_2 (101).

band minimum (CBM), the value of 2.9 eV is consistent with expectations. It suggests that the Fermi level lies ~0.3±0.1 eV below the CBM for the anatase TiO_2 (101) surface studied here. This position depends strongly on defect concentration, but comparative photoemission measurements of anatase and rutile show that the gap between the Fermi level and the CBM is significantly larger (by at least 0.1 eV) at the anatase (101) surface than for the crystallographically equivalent rutile (110) surface.[43] The band gap for bulk CuI has been measured as 3.1 eV.[44] CuI is a *p*-type material, and the acceptor levels created by the presence of excess I^- anions are thought to lie in the band gap near the VBM. For CuI we therefore expect that the VBM, in principle, should lie quite close to the Fermi level in energy, as is observed.

Following Eq. (1), the core level binding energy difference and other parameters can be calculated and are shown below. After a total of 30 min dosing, where we estimate the CuI overlayer thickness to be 4±1 Å (denoted by coverage Θ_{30}), we find $\Delta BE_{CL}^{s/f}(\Theta_{30})=50.9-37.3=13.6\pm0.1$ eV. Here we have taken as core levels I $4d_{3/2}$ for the overlayer film and Ti $3p$ for the substrate. We obtain $(BE_{CL}^{S}-BE_{VBM}^{S})=37.8-2.9=34.9\pm0.1$ eV and $(BE_{CL}^{f}-BE_{VBM}^{f})=50.6-0.5=50.1\pm0.1$ eV, where we use the I $4d_{3/2}$ CL BE for a thick (>40 Å) film of CuI deposited on TiO_2. Using Eq. (1), the valence band offset at the interface, $\Delta E_V^{s/f}(\Theta_{30})$, is found to be −1.6±0.2 eV. Here, the minus sign in the result indicates that the valence band of CuI lies above that of TiO_2 as expected. The conduction band offset, $\Delta E_C^{s/f}(\Theta_{30})$, at the interface calculated using Eq. (2) is found to be −1.5±0.2 eV.

The presence of a possible interface dipole (ID) can be evaluated with a knowledge of the work function of each material. This requires SEED edge measurements for both the substrate and the overlayer. The value of 4.7±0.1 eV obtained for the work function of the anatase single crystal (101) surface (Fig. 2) is in reasonable agreement with values reported earlier for TiO_2 nanoparticulate thin films.[45] The value calculated for the work function of CuI is 5.4±0.1 eV. There are no earlier reports of work function measurements for CuI with which to compare this result. Nevertheless, in a broad sense, the difference in workfunctions between *n*-type and *p*-type electrodes is considered to be equal to the open circuit photovoltage that can be extracted from a heterojunction solar cell.[46] The difference in work functions between CuI and anatase TiO_2 as calculated here is equal to 0.7±0.1 eV. Open circuit photovoltage (V_{oc}) values currently being observed with solid state dye-sensitized solar cells where anatase-phase TiO_2 and CuI are used as electron and hole-conducting materials, respectively, lie in the range of 500–550 mV (e.g., Ref. 14 and references therein). The work function difference between anatase TiO_2 and CuI observed here is thus approximately equal to the experimentally observed V_{oc} values and suggests that the work function derived for CuI is reasonably accurate. The work functions may then be used to evaluate the ID for this interface following a previously published method, which compares the difference in work function between the overlayer and the substrate with the measured total band bending.[17,34] This gives a value for the ID of 0.7−0.8 eV=−0.1±0.2 eV, i.e., there is no detectable interface dipole at this interface, within the limits of experimental error.

Thus our results indicate that the energy lineup at the

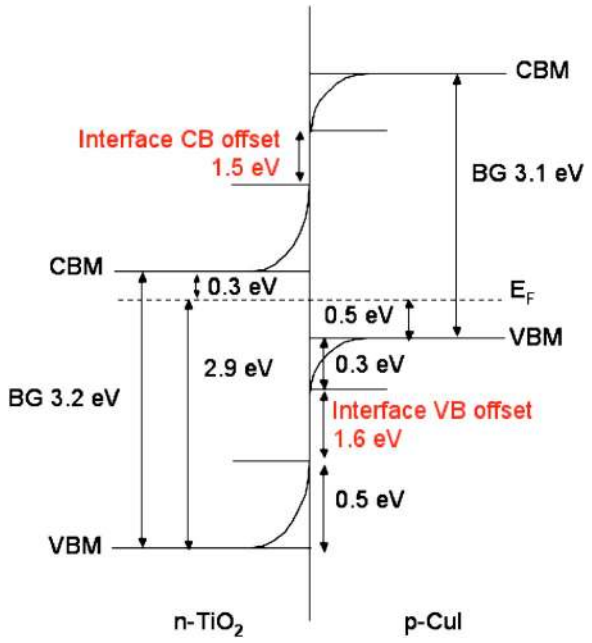

FIG. 5. Band energy alignment at the heterojunction interface of single crystal anatase-phase *n*-TiO_2 (101) and *p*-CuI, after 30 min CuI deposition (corresponding to around 4 Å layer thickness, see text). The diagram is constructed using the experimentally observed core level binding energy shifts for the anatase TiO_2 substrate (Ti 3*p* core level shift between the clean surface and 30 min CuI dose) and the CuI overlayer [I 4*d* core level shift between 30 min CuI dose and a thick (>40 Å) film of CuI on anatase TiO_2], the VBMs for clean anatase TiO_2 (101) and CuI determined by the method shown in Figs. 4(a) and 4(b), and also using reported band gap values for anatase TiO_2 and CuI (Refs. 15, 16, 28, 44, and 47). The figure is not drawn to scale.

TiO_2/CuI heterojunction interface may be accounted for by band bending at the interface with a negligible interface dipole. This contrasts with the behavior of inorganic/organic heterojunctions, where typically no band bending is observed at the interface, but there is usually an ID.[18,19,34] Figure 5 shows the resulting band energy lineup at the interface between the TiO_2 (101) surface and CuI. This diagram was constructed using the core level BE shifts observed experimentally, the experimental VBMs, and the reported band gaps for each material [TiO_2=3.2 eV (Refs. 28 and 47) and CuI=3.1 eV (Ref. 44)]. As can be seen in the diagram, the resulting interface valence band and conduction band offsets are −1.6±0.2 and −1.5±0.2 eV, respectively.

C. The nanoparticulate anatase TiO_2/CuI interface

The Ti 3*p* core level spectrum for an as-presented and CuI-dosed nanoparticulate thin film of anatase-phase TiO_2 (with an average particle size of 7.3 nm) is shown in Fig. 6(a). In general, the "as-presented" spectrum is very similar to that recorded from the clean single crystal (101) surface, although the signal-to-noise level is worse. For that reason, the spectra in Fig. 6(a) have been subjected to a low-level binomial smoothing process, which has reduced the background noise level by around 30%. (This is in contrast to all other spectra presented here, which are presented without any spectral smoothing.) Following the deposition of CuI, the Ti 3*p* peak of the as-prepared film shifts to lower BE. After 10 min CuI dosing, there is no increase in FWHM of the Ti 3*p* feature. However, after 90 min deposition, the Ti 3*p* peak shape appears to be broadened at the high binding energy side (around 41 eV BE). This part of the Ti 3*p* peak structure has been previously associated with surface Ti species having a different coordination environment to the bulk,[26] and the increase in intensity here on deposition may indicate a more significant chemical reaction between the as-presented anatase nanoparticles and CuI than in the case of the single crystal substrate. However, given the poor signal-to-noise level in these spectra, this conclusion must be tentative. The BE shift of the Ti 3*p* peak of the nanoparticulate film following the deposition of CuI is 0.3±0.1 eV, smaller than that observed for the anatase single crystal (101) surface (0.5 eV). This implies that the band bending is smaller in the nanoparticulate TiO_2 thin film than in the bulk material. In general, this agrees with the idea that the size of the nanoparticles themselves constrains the dimension of the depletion layer that may be maintained at the interface, hence smaller band-bending effects are expected.[48] We investigate this hypothesis further in Sec. III E. A longer dosing time than anticipated (nearly three times longer than for the single crystal surface) was required in order to reach a state where the valence band spectra of the dosed nanoparticulate surface showed clear features from both the substrate and the overlayer (see Fig. 7), suggesting that CuI may be filling some of the voids in the nanoparticulate film. Using the method described in Sec. II, we estimate the amount of material deposited to be equivalent to that needed to yield a uniform overlayer of thickness of 6±1 Å (about 1 unit cell or two atomic layers of CuI) if deposited on a single crystal. However, the deposition is clearly far less uniform than that observed on the single crystal surface, as attenuation of the Ti 3*p* peak on dosing [Fig. 6(a)] is much smaller than that observed for the single crystal surface [Fig. 1(a)]. Given that CuI deposition (albeit at higher temperatures than those used here) may produce three-dimensional clusters with dimensions up to tens of nanometers,[27] the CuI film may not be conformal across the whole TiO_2 surface.

The I 4*d* core level photoemission spectra obtained following dosing are shown in Fig. 6(b). As can be seen, after 90 min CuI dosing, the I 4*d* doublet shifts to lower BE by 0.4±0.1 eV, 0.2 eV different from a bulk CuI film (BE of 50.6 eV). Within experimental error, this is similar to the difference observed on dosing the anatase single crystal (101) surface, indicating that the band bending in the CuI layer is similar in both experiments. On increased dosing, the FWHM of these features decreases (for example, the FWHM of the I $4d_{5/2}$ feature narrows by almost 0.3 eV between 10 and 90 min dosing times). If we assume that the spectra at low dosing times are most sensitive to I species bonded to the anatase surface (as opposed to I species in bulk CuI at long deposition times), this may indicate some chemical interaction between the CuI and the as-presented nanoparticulate anatase surface (as inferred from the Ti 3*p* spectra).

Figure 7 shows the valence band spectra of the as-presented nanoparticulate TiO_2 surface with increasing levels of CuI dosing. The valence band spectrum of the as-prepared nanoparticulate TiO_2 agrees well with previous ultraviolet photoemission spectroscopy measurements on nanocrystal-

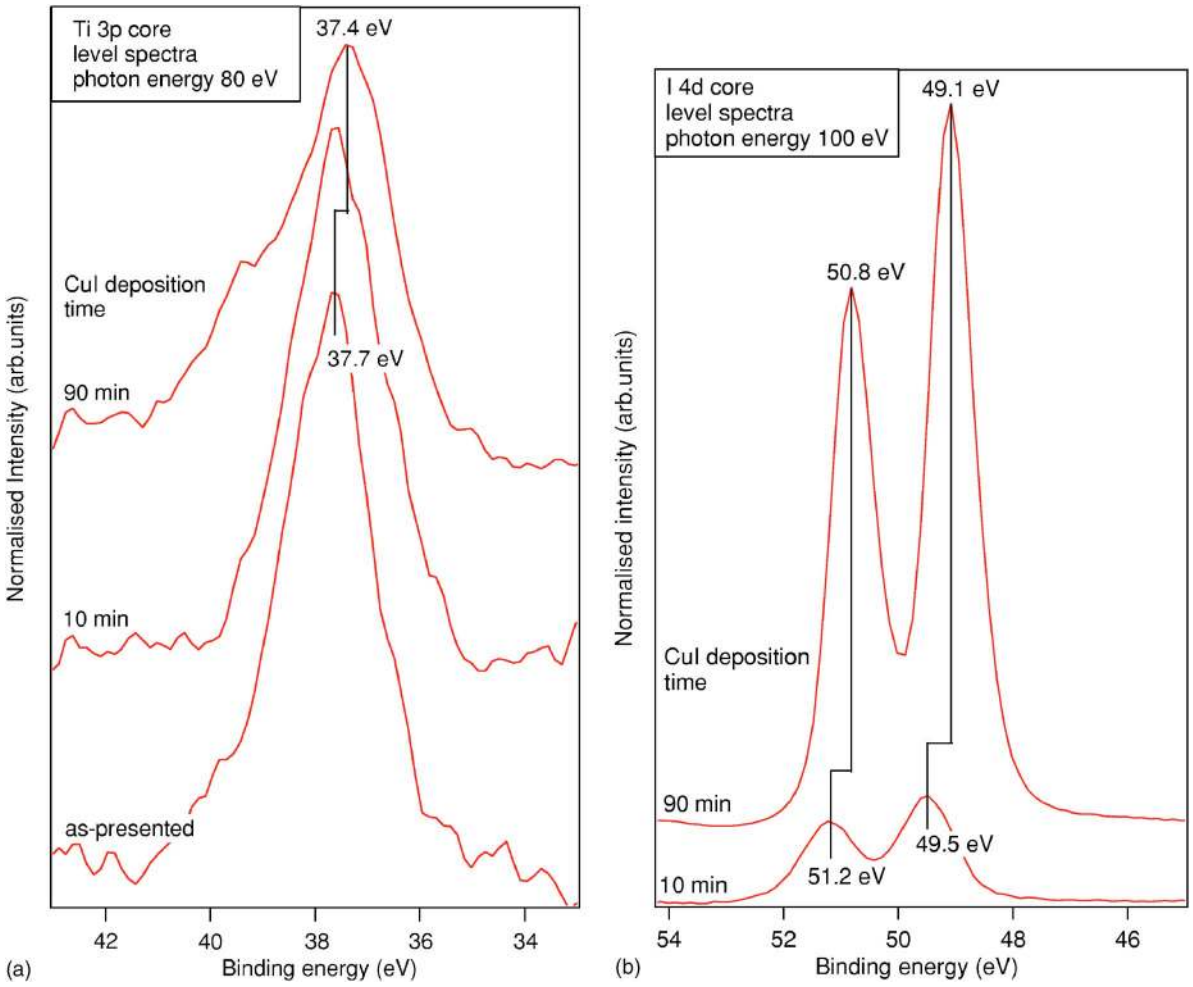

FIG. 6. Core level spectra recorded for an as-presented nanoparticulate anatase TiO_2 thin film (of average particle size of 7.3 nm) before and after CuI dosing at different dosing intervals. (a) Ti 3*p* core level spectra. A binomial smoothing routine has been applied (reducing the background noise level by around 30%). (b) I 4*d* core level spectra.

line TiO_2 thin films observed using a He II excitation source[49] and is also in good agreement with the valence band spectrum of the clean anatase single crystal (101) surface shown in Fig. 3. The valence band widths of both are very similar, although the separate features due to O 2*p*-Ti 3*d* σ-bonding states (at 7.6±0.1 eV BE) and Ti 3*d*-O 2*p* π-bonding states (the shoulder at around 5 eV BE) are not so well resolved in the spectrum of the nanoparticulate thin film. The lower intensity of the defect state (at around 1 eV BE) in the case of the nanoparticulate surface indicates that this surface has fewer defects than the single crystal surface. This can be expected as this surface was not subjected to any surface etching or annealing procedure that would create defects prior to the photoemission experiment. The intensity of the defect peak observed in this sample reflects the intrinsic defect concentration in the as-presented nanoparticulate film. Upon dosing for 90 min, the higher BE feature in the valence band is shifted to lower BE by 0.4±0.1 eV, which is (within the error bounds) similar to that observed for the single crystal surface. In addition, the valence band is widened at its lower BE side following CuI dosing with the introduction of the three new features in the band gap region of the nanoparticulate TiO_2 that were observed in the single crystal case (Sec. III A) at 2.2±0.1, 3.4±0.1, and 4.8±0.1 eV BE. The CuI valence band features at 2.2±0.1 and 3.4±0.1 eV are shifted to higher BE by 0.3–0.4 eV from those in the bulk CuI pellet (Fig. 3). This value is reasonably consistent with the shift in the I $4d_{3/2}$ feature discussed above.

Figure 8 displays SEED edge spectra for the as-presented and dosed nanoparticulate TiO_2 surfaces. This yields a value for the work function for the nanoparticulate thin film of 4.5±0.1 eV, which is 0.2 eV smaller than that for the clean single crystal (101) surface. A similar difference has been observed between sputtered and unsputtered nanoparticulate TiO_2 thin films and has been explained as arising from the influence of surface states or surface contamination on the as-presented film.[45,49] The difference in work function observed here is likely to have a similar origin as repeated sputtering and annealing steps were used in UHV to clean the anatase single crystal (101) surface, whereas the nanoparticulate sample was studied in the as-presented state, without any sputtering or annealing. Upon dosing, the SEED edge for the nanoparticulate TiO_2 film shifts toward lower BE resulting in a 1.2±0.1 eV BE shift after a total of 90 min dose. This is 0.5±0.1 eV higher than that observed for the single crystal (101) surface. It corresponds to a shift to an apparent work function of 5.7±0.1 eV, 0.3 eV larger than the work function estimated earlier for a thick film of CuI. This sug-

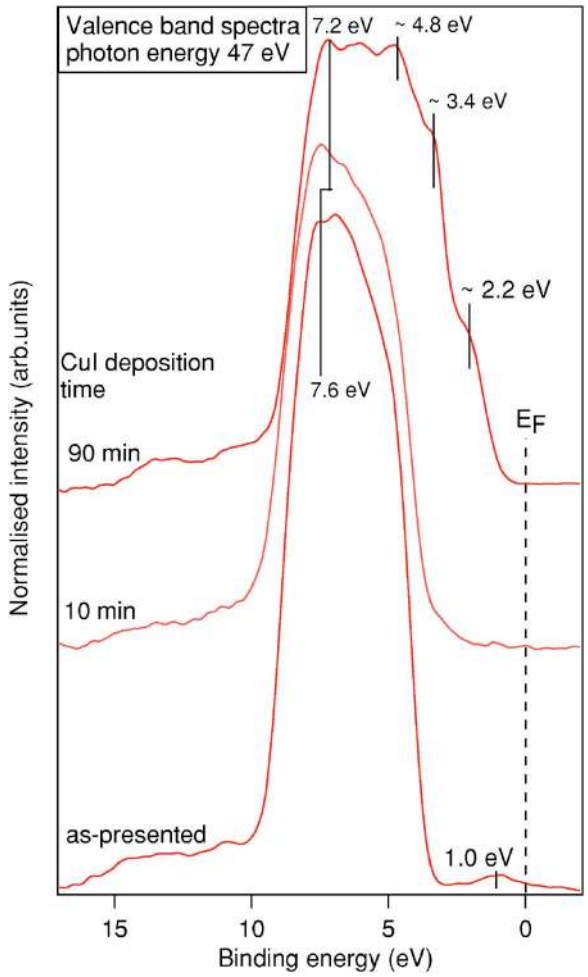

FIG. 7. Valence band EDCs for an as-presented nanoparticulate anatase TiO_2 thin film (of average particle size of 7.3 nm) before and after CuI dosing at different dosing intervals. Dosing intervals are as in Fig. 6.

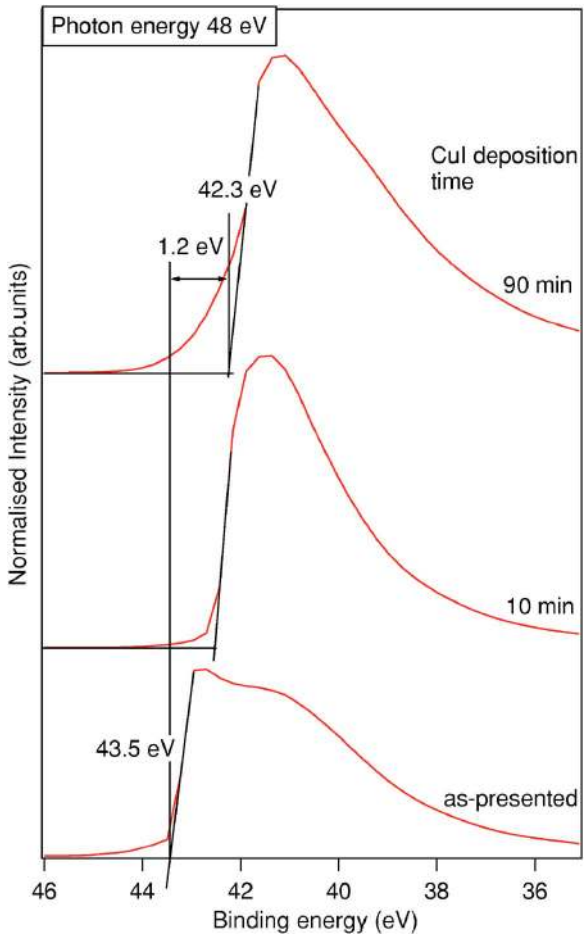

FIG. 8. SEED spectra recorded for an as-presented nanoparticulate anatase TiO_2 thin film (of average particle size of 7.3 nm) before and after CuI dosing at different dosing intervals. Dosing intervals are as in Fig. 6. The spectra were recorded while applying a negative bias of −37.9 eV to the sample; this has been accounted for in aligning the spectra on a binding energy scale. The method used to determine the SEED edge position is described in the text and is shown in the figure (Ref. 34).

gests that there may be an interface dipole at this interface. This is considered further in the next section.

D. Band energy alignment at the nanoparticulate anatase TiO_2/CuI interface

The energy band alignment at the interface for the nanoparticulate TiO_2/CuI interface can be carried out by the same method used for the anatase single crystal (101)/CuI interface previously. Again, for this purpose, determination of VBMs of the substrate (the nanoparticulate TiO_2 film) and the overlayer are required. The latter is taken from the VBM for a thick (>40 Å) film of CuI on the anatase TiO_2 single crystal (101) surface determined previously. The VBM of the as-presented nanoparticulate TiO_2 thin film was determined using the method outlined in Sec. III B. A value of 3.1±0.1 eV for the VBM was extracted. This is 0.2±0.1 eV higher than that observed for the single crystal (101) surface (2.9±0.1 eV). The higher VBM position for the nanoparticulate TiO_2 sample is expected, reflecting the larger band gap compared with the bulk material.

Figure 9 shows a possible band energy alignment at the interface for the nanoparticulate TiO_2/CuI system. As in the case of single crystal (101)/CuI interface, this energy level diagram was constructed using Ti 3*p* and I 4*d* core level binding energy shifts, VBMs, and the band gaps of each material. The band gap for the nanoparticulate TiO_2 (with an average particle size of 7.3 nm) was estimated from information available for the band gap values of TiO_2 nanoparticles with different particle sizes.[50,51] The estimated value for the band gap of the nanoparticulate TiO_2 is about 3.4 eV, compared with a bulk band gap of 3.2 eV.[28,47] This is consistent with the magnitude of the shift observed in the VBM of 0.2 eV between the nanoparticle and single crystal samples. Figure 9, in combination with Eqs. (1) and (2), yields a valence band offset of −2.1±0.2 eV and a conduction band offset of −1.8±0.2 eV, both significantly larger than in the single crystal case. Comparison of the difference in work function between the overlayer and the substrate with the measured total band bending now gives a value for the ID of 0.9−0.5 eV=0.4±0.2 eV, i.e., there appears to be a significant interface dipole at the interface between nanoparticulate anatase-phase TiO_2 and CuI.

E. Discussion

It is clear that both the single crystal and the nanoparticulate junctions show an energy level lineup consistent with

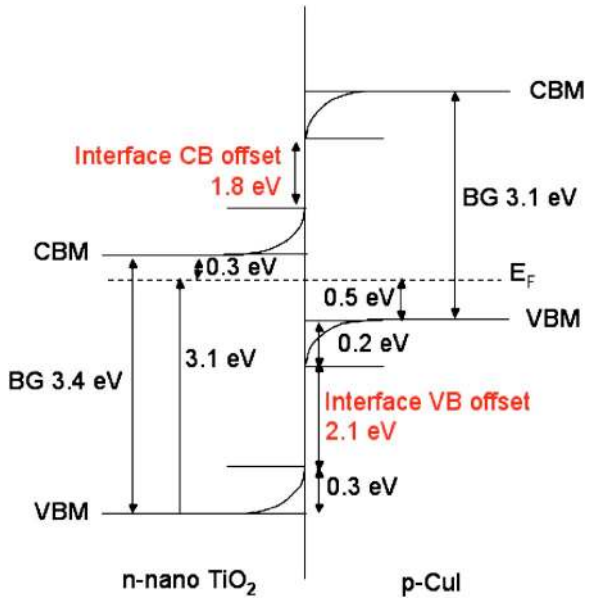

FIG. 9. Band energy alignment at the heterojunction interface for an as-presented nanoparticulate anatase-phase *n*-TiO_2 thin film (of average particle size of 7.3 nm) and *p*-CuI. The diagram shows the alignment after 90 min CuI deposition (equivalent to around 6 Å layer thickness if uniformly deposited, see text). The diagram is constructed using experimentally observed core level binding energy shifts for the anatase TiO_2 substrate (Ti 3*p* core level shift between the clean surface and 90 min CuI dose) and the CuI overlayer [I 4*d* core level shift between 90 min CuI dose and a thick (>40 Å) film of CuI on anatase TiO_2], the VBMs for the as-presented nanoparticulate *n*-anatase TiO_2 thin film (see text) and CuI [Fig 4(b)] and also using band gap values for the nanoparticulate anatase TiO_2 thin film (extrapolated, see text) and CuI (Refs. 15, 16, and 44). The figure is not drawn to scale.

p-n junction formation. In both cases, our experiments suggest that the conduction band minimum and the VBM are lower on the *n*-TiO_2 side of the interface than on the *p*-CuI side, i.e., that the junction is a type-II heterojunction, with unimpeded transport of electrons to the lower side, as required for high efficiency in a photovoltaic device. In both cases, significant band bending is observed at the interface in both *n*- and *p*-type materials. This contrasts with the behavior of liquid-electrolyte dye-sensitized solar cell devices, where flatband behavior is anticipated—largely on the basis of the surface screening provided by the electrolyte (for example, hydration of the TiO_2 surface), but also on the assumption that the nanoparticulate morphology of the anatase phase should not permit the maintenance of a substantial depletion layer at the interface.[48] In contrast, we have measured significant band bending in the solid state nanoparticulate junction. The energy level lineup at the crystalline and nanoparticulate *p-n* junctions has been measured for two slightly different sets of deposition conditions (in terms of the amount of CuI deposited). The properties of the *p-n* junction, for example, the valence and conduction band offsets, are clearly functions of coverage [Eqs. (1) and (2)]. Nevertheless, it seems to be the case that the band bending observed in nanoparticulate TiO_2 is smaller than that observed in the single crystal system, and this may reflect the fact that the depletion layer in the nanoparticle system is typically constrained in extent to the average radius of the particles (in our case around 3.6 nm). In order to investigate this hypothesis, we estimate the depletion layer widths in our experiments below.

A simple estimate of the depletion layer width may be obtained from solution of Poisson's equation[52] as

$$d = [2\varepsilon_0\varepsilon_r V/(n_d e)]^{1/2}, \tag{3}$$

where ε_0 is the permittivity of free space, ε_r is the relative dielectric constant of the medium (in this case the static dielectric constant), V is the band bending at the interface, n_d is the carrier concentration, and e is the electronic charge. For a typical semiconductor with $\varepsilon_r = 10$, $V = 1$ V, and $n_d = 10^{17}$ cm^{-3}, this gives $d = 100$ nm.[52] However, for some oxide materials such as TiO_{2-x}, which are intrinsically nonstoichiometric, the concentration of carriers (originating from oxygen defects) may be several orders of magnitude larger than is typical in a "conventional" semiconductor material, leading to significantly smaller depletion layer widths [Eq. (3)].

We begin by estimating the carrier concentration in the single crystal anatase sample used to make the heterojunction shown in Fig. 5. The photoemission spectrum of this surface prior to deposition (Fig. 3) indicates that the surface is highly defected (as indicated by the strong 'defect' peak at around 1 eV BE). The majority of these defects are created by the cycles of bombardment and annealing used to obtain an uncontaminated surface.[43] The defect concentration is therefore expected to be considerably greater than would be anticipated under normal cell operating conditions. We have recently used synchrotron radiation–excited core level photoemission to estimate the concentration of oxygen vacancies as a function of surface treatment at this and a number of other anatase and rutile surfaces.[43] The concentration of oxygen vacancies, and the way in which it varies with surface treatment on the rutile (110) surface has also been characterized by high-resolution scanning tunneling microscopy (STM).[53] In the present case, we obtain an oxygen vacancy concentration at the surface of the anatase (101) surface following Ar^+ ion bombardment and annealing of $7 \pm 2\%$,[43] which, as one oxygen defect has two defect electrons associated with it, corresponds to around $15 \pm 2\%$ of the Ti^{4+} ions at the surface reduced to Ti^{3+}—in other words the surface is grossly nonstoichiometric. These estimates are consistent with those obtained from STM for similarly treated surfaces.[53] Using available crystallographic data,[54] we can then obtain an estimate of the density of defect electrons, N_d (101) in the surface layer of the anatase (101) sample of 4.4×10^{21} cm^{-3}. As expected, this is substantially larger than the concentration of defects in, say, a doped III-V semiconductor material, and the calculated depletion layer width will be correspondingly much smaller. In order to estimate this, we require the band bending in the single crystal TiO_2 at the interface, estimated as 0.5 V from our experiments (Fig. 5), and an estimate of the static dielectric constant of bulk anatase-phase TiO_2. The latter is rather problematic, as values given in the literature vary widely, and will be affected by defect concentration. We have chosen to take $\varepsilon_r = 48$.[55] This lies in the midrange of quoted values, but as literature values vary by around an order of magnitude, we note that

the resulting value of the depletion layer width (8 Å) is a rough estimate only, and the value may lie in the range of 3–12 Å. Nevertheless, it is clear that the depletion layer width at the single crystal anatase surface is very small due to the high defect concentration. It is conveniently probed by surface sensitive techniques such as photoemission, as it rather shorter than the typical sampling depth of the technique in these samples (which is itself a function of photon energy, but is typically some tens of angstroms).

In the case of the nanocrystalline junction, where CuI is deposited on an as-presented nanocrystalline anatase thin film, it is clear from Fig. 7 that the concentration of defects at the anatase surface is much smaller than for the Ar^+-etched single crystal surface; nevertheless, a significant concentration of defects is present, as evidenced by the "defect" peak at around 1 eV BE. In this case the sample is studied in the as-presented state, without any etching or annealing treatment and was not heated during dosing. The surface is stable to oxygen loss in UHV. In this case, the intensity of the defect peak is indicative of the intrinsic concentration of defects at the surface of the nanoparticulate sample. By comparison with Ref. 43, we estimate that the concentration of surface oxygen vacancies is $1\pm2\%$ or rather less, corresponding to a maximum defect electron density $N_d nc$ in the surface layer of the nanocrystalline anatase sample of 5.9×10^{20} cm^{-3}, a value still considerably larger than is typical for a conventional semiconductor. In this case, the measured band bending in the anatase thin film is 0.3 V. We note that the particle size in the nanoparticulate film is rather smaller than that typically encountered in dye-sensitized photovoltaic devices [around 15 nm (Ref. 48)]. The trap density in these samples has been shown to be proportional to the internal surface area,[56] so the defect electron density observed here may be larger than that typically found in real devices. Again, literature estimates for the static dielectric constant of as-deposited nanocrystalline anatase thin films vary considerably.[57] For convenience, we again use the value of $\varepsilon_r=48$ for bulk anatase,[55] as this lies in the midrange of quoted values for as-deposited thin films [which are typically in the range of 30—80 (Ref. 57)]. We obtain an estimate for the depletion layer width in the nanocrystalline anatase sample of around 1.6 nm, with a similar caveat to the single crystal case, that the value may lie in the range of 1.4–2.6 nm. This value is rather larger than that obtained in the single crystal case due to the difference in carrier concentration. It is nevertheless of a similar magnitude (in fact, rather smaller than) the average radius of a nanoparticle in the anatase thin film (around 3.6 nm). Thus we conclude that although we measure significant band bending in the nanocrystalline anatase thin film, the depletion layer width maintained by this voltage is small enough to be contained within the dimension of the nanoparticles making up the film.

In the case of the single crystal anatase (101) interface, we find that the electron affinity rule (EAR) of Anderson is obeyed,[58] i.e., there is a negligibly small interface dipole (of -0.1 ± 0.2 eV), and the overall band bending at the junction matches the work function difference. The EAR rule does not hold precisely in many experimentally investigated heterostructures,[17] and indeed, in the case of the nanocrystalline thin film interface, we observe a significant interface dipole of 0.4 ± 0.2 eV. Here the work function difference is not completely accounted for by the measured band bending. Although our estimates show that the band bending within the nanoparticulate thin film is close to being constrained by the dimensions of the nanoparticles in the film, the reasons for the significant interface dipole are not completely clear. However, we anticipate that a discontinuity in the electric field at the interface may arise due to the roughness of the nanocrystalline morphology, due to chemical reaction at the interface suggested by the core level photoemission measurements (Sec. III C), or due to the presence of residual foreign atoms from the solution phase preparation route, all of which are absent in the case of the atomically flat and clean single crystal surface. The surface species might be expected to include surface hydroxyl, water, and possibly residual organic material from the isopropanol used in the final precipitation. Such species typically give rise to features to the high binding energy side of the valence band, particularly at around 10 eV BE.[59] The absence of strong features due to contamination in the valence band spectra of the nanoparticulate film (Fig. 7) suggests that this contamination is not severe. Perhaps a more important cause of an interface dipole might be the presence at the interface of polar anatase surfaces. By analogy with rutile,[59] the (101) surface of anatase should not be a polar surface (i.e., it should have no dipole normal to the surface). This is consistent with the absence of an interface dipole in the single crystal case. In contrast, in the nanoparticulate samples, a range of surface terminations would be expected at the surfaces of the nanoparticles, including (101), (001), and others, and some of these are likely to possess an intrinsic surface dipole that could contribute to the observed interface dipole.

IV. CONCLUSIONS

Photoemission has been used to determine the energy level lineup at the interface between vacuum-deposited CuI and both single crystal and nanoparticulate TiO_2. We conclude that both interfaces are type-II heterojunction interfaces, allowing unimpeded transport of electrons into the TiO_2 layer. Band bending is observed at both junctions, and in the case of the single crystal system, work function measurements suggest there is a negligible interface dipole, i.e., the EAR (Ref. 58) is obeyed and the band bending at the junction matches the work function difference. The behavior of this inorganic/inorganic interface thus contrasts with that typically observed at inorganic/organic heterojunctions.[18,19,34] Smaller band bending is observed in the nanoparticulate TiO_2 film than in the single crystal sample. This is consistent with the idea that in the nanoparticulate sample the sustainable depletion layer depth is constrained by the dimension of the nanoparticles. However, we show that (because of the relatively high carrier concentrations in the nanoparticles), a significant voltage is required to maintain a rather small depletion layer. In the case of the nanoparticulate thin film, our measured band bending corresponds to a depletion layer depth of only around 2 nm, compared with an average nanoparticle radius of 3.6 nm. It is thus clear

that significant band bending may be maintained even in nanoparticulate anatase. The measured energy level lineup at the TiO_2/CuI interface is thus rather different from the "flatband" picture often assumed for dye-sensitized solar cell systems. In the nanoparticulate system the calculated valence and conduction band offsets are larger than for the single crystal case, the band bending is no longer large enough to account for the difference in work function, and a substantial interface dipole of 0.4 ± 0.2 eV is found. This may be due to the presence of polar surfaces, foreign atoms, chemical reaction, or surface roughness at this interface, and contrasts with the behavior found at the atomically flat and clean nonpolar single crystal interface.

Photoemission, which has a sampling depth similar to the probed depletion layer widths, is a powerful method for direct determination of the energy level lineup at *p-n* junctions. The band offset at a heterojunction interface is one of the most important properties of the junction and is important in optimizing the photoconversion yield of the cell. In this case we have directly measured the VB and CB offsets, demonstrated the presence of substantial band bending, and, in the nanoparticulate case, measured a significant interface dipole. The resulting energy level lineup cannot be predicted from flatband potential measurements widely used for dye-sensitized solid state solar cell materials. In principle, accurate determination of the energy level lineup at this heterojunction could help us guide the choice of sensitizing dye for optimum interface charge transfer. Work aimed at understanding how the energy level lineup is affected by dye adsorption is underway.

ACKNOWLEDGMENTS

This work was funded by EPSRC (UK) under Grant Nos. GR/S07131 and GR/R97795 and CCLRC (UK). The authors thank Professor D. A. Evans for a number of useful discussions.

[1] B. O'Regan and M. Grätzel, Nature (London) **353**, 737 (1991).
[2] M. Grätzel, J. Photochem. Photobiol., A **164**, 3 (2004); Inorg. Chem. **44**, 6841 (2005).
[3] M. K. Nazeeruddin, A. Kay, I. Rodicio, R. Humphry-Baker, E. Muller, P. Liska, N. Vlachopoulos, and M. Grätzel, J. Am. Chem. Soc. **115**, 6382 (1993).
[4] M. Law, E. L. Greene, C. J. Johnson, R. Saykally, and P. Yang, Nat. Mater. **4**, 455 (2005).
[5] K. Tennakone, G. R. R. A. Kumara, I. R. M. Kottegoda, and V. P. S. Perera, Chem. Commun. (Cambridge) **1999**, 15.
[6] M. A. Green, Physica E (Amsterdam) **14**, 11 (2002).
[7] A. R. Kumarasinghe and W. R. Flavell, Physica E (Amsterdam) **14**, 224 (2002).
[8] F. Cao, G. Oskam, and P. C. Searson, J. Phys. Chem. **99**, 17071 (1995).
[9] K. Murakoshi, R. Kogure, Y. Wada, and S. Yanagida, Sol. Energy Mater. Sol. Cells **55**, 113 (1998).
[10] M. Matsumoto, H. Miyazaki, K. Matsuhiro, Y. Kumashiro, and Y. Takaoka, Solid State Ionics **89**, 263 (1996).
[11] U. Bach, D. Lupo, P. Comte, J. E. Moser, F. Weissörtel, J. Salbeck, H. Spreitzer, and M. Grätzel, Nature (London) **395**, 583 (1998).
[12] K. Tennakone, G. R. R. A. Kumara, A. R. Kumarasinghe, K. G. U. Wijayantha, and P. M. Sirimanne, Semicond. Sci. Technol. **10**, 1689 (1995).
[13] B. O'Regan, F. Lenzmann, R. Muis, and J. Wienke, Chem. Mater. **14**, 5023 (2002).
[14] T. Taguchi, X. Zhang, I. Sunanto, K. Tokuhiro, T. N. Rao, H. Watanabe, T. Nakamori, M. Uragami, and A. Fujishima, Chem. Commun. (Cambridge) **2003**, 2480.
[15] B. Bouhafs, H. Heireche, W. Sekkal, H. Aourag, and M. Certier, Phys. Lett. A **240**, 257 (1998).
[16] W. Sekkal and A. Zaoui, Physica B **315**, 201 (2002).
[17] G. Liu, T. Schulmeyer, J. Brötz, A. Klein, and W. Jaegermann, Thin Solid Films **431–432**, 477 (2003).
[18] D. A. Evans, H. J. Steiner, A. R. Vearey-Roberts *et al.*, Appl. Surf. Sci. **212–213**, 417 (2003) and references therein.
[19] D. A. Evans, H. J. Steiner, A. R. Vearey-Roberts *et al.*, Nucl. Instrum. Methods Phys. Res. B **199**, 475 (2003).
[20] T. Chasse, C.-I. Wu, G. Hill, and A. Khan, J. Appl. Phys. **85**, 6589 (1999).
[21] Y. Hirose, W. Chen, E. I. Haskal, S. R. Forrest, and A. Kahn, Appl. Phys. Lett. **64**, 3482 (1994).
[22] O. Lang, A. Klein, C. Pettenkofer, W. J. Jaegermann, and A. Chevy, J. Appl. Phys. **80**, 3817 (1996).
[23] A. Klein, T. Löher, Y. Tomm, C. Pettenkofer, and W. J. Jaegermann, Appl. Phys. Lett. **70**, 1299 (1997).
[24] K. Horn, M. Moreno, M. Alonso, M. Höricke, R. Hey, J. L. Sacedón, and K. H. Ploog, Vacuum **67**, 115 (2002).
[25] N. Nakayama, T. Kuramachi, T. Tanbo, H. Ueba, and C. Tatsuyama, Surf. Sci. **244**, 58 (1991).
[26] A. G. Thomas, W. R. Flavell, C. Chatwin, S. Rayner, T. Tsoutsou, A. R. Kumarasinghe, D. Brete, T. K. Johal, S. Patel, and J. Purton, Surf. Sci. **59**, 159 (2005).
[27] P. G. Karlsson, S. Bolik, J. H. Richter, B. Mahrov, E. M. J. Johansson, J. Blomquist, P. Uvdal, H. Rensmo, H. Siegbahn, and A. Sandell, J. Chem. Phys. **120**, 11224 (2004).
[28] L. Kavan, M. Grätzel, S. E. Gilbert, C. Klemenz, and H. J. Scheel, J. Am. Chem. Soc. **118**, 6716 (1996).
[29] R. Hengerer, B. Bolliger, E. Erbudak, and M. Grätzel, Surf. Sci. **162**, 460 (2000).
[30] See, e.g., J. W. Campbell, J. Appl. Crystallogr. **28**, 228 (1995).
[31] A. G. Thomas, W. R. Flavell, A. R. Kumarasinghe, A. K. Mallick, D. Tsoutsou, G. C. Smith, R. Stockbauer, S. Patel, M. Grätzel, and R. Hengerer, Phys. Rev. B **67**, 035110 (2003).
[32] P. Christian (unpublished).
[33] A. K. Mallick, Ph.D Thesis, The University of Manchester, 2005.
[34] T. U. Kampen, G. Gavrila, H. Mendez, D. R. T. Zahn, A. R. Vearey-Roberts, D. A. Evans, J. W. Wells, I. T. McGovern, and W. Braun, J. Phys.: Condens. Matter **15**, S2679 (2003).
[35] R. Sanjines, H. Tang, H. Berger, F. Gozzo, G. Margaritondo, and F. Levy, J. Appl. Phys. **75**, 2945 (1994).
[36] Z. Zhang, S.-P. Jeng, and V. E. Henrich, Phys. Rev. B **43**, 12004 (1991).
[37] R. Asahi, Y. Taga, W. Mannstadt, and A. J. Freeman, Phys. Rev. B **61**, 7459 (2000).
[38] *Heterojunction Band Discontinuities*, edited by F. Capasso and G. Margaritondo (North Holland, Amsterdam, 1987).
[39] D. A. Keen and S. Hull, J. Phys.: Condens. Matter **7**, 5793 (1995).
[40] T. Ishii, M. Taniguchi, and A. Kakizaki, Phys. Rev. B **33**, 5664 (1986).
[41] B. Mahrov, G. Boschloo, A. Hagfeldt, H. Siegbahn, and H. Rensmo, J. Phys. Chem. B **108**, 11604 (2004).
[42] S. Kono, T. Sagawa, T. Kobayashi, and T. Ishii, Phys. Rev. Lett. **28**, 1385 (1972).
[43] A. G. Thomas, W. R. Flavell, A. K. Mallick *et al.*, Phys. Rev. B **75**, 035105 (2007).
[44] P. M. Sirimanne, M. Rusop, T. Shirata, T. Soga, and T. Jimbo, Chem. Phys. Lett. **366**, 485 (2002).
[45] G. Liu, W. Jaegermann, J. He, V. Sundström, and L. Sun, J. Phys. Chem. B **106**, 5814 (2002).
[46] For example, M. C. Scharber, D. Mühlbacher, M. Koppe, P. Denk, C. Waldauf, A. J. Heeger, and C. J. Brabec, Adv. Mater. (Weinheim, Ger.) **18**, 789 (2006).
[47] R. Hengerer, Ph.D Thesis, Ecole Polytechnique Federale De Lausanne, 2000.
[48] A. Hagfeldt and M. Grätzel, Chem. Rev. (Washington, D.C.) **95**, 49 (1995).
[49] A. Orendorz, J. Wüsten, C. Ziegler, and H. Gnaser, Appl. Surf. Sci. **252**, 85 (2005).
[50] G. Luis, C. Rego, and S. V. Batista, J. Am. Chem. Soc. **125**, 7989 (2003).
[51] C. Korman, D. W. Bahnemann, and M. R. Hofman, J. Phys. Chem. **92**, 5196 (1998).
[52] P. A. Cox, *The Electronic Structure and Chemistry of Solids* (Oxford University Press, Oxford, 1987), p. 236.

[53] S. Wendt, R. Schaub, J. Matthiesen *et al.*, Surf. Sci. **598**, 226 (2005).
[54] D. T. Cromer and K. Herrington, J. Am. Chem. Soc. **77**, 4708 (1955).
[55] R. J. H. Clark, *The Chemistry of Titanium and Vanadium. An Introduction to the Chemistry of the Early Transition Elements* (Elsevier, New York, 1968), p. 270.
[56] N. Kopidakis, N. R. Neale, K. Zhu, J. van de Lagemaat, and A. J. Frank, Appl. Phys. Lett. **87**, 202106 (2005).
[57] W. Yang, J. Marino, A. Monson, and C. A. Wolden, Semicond. Sci. Technol. **21**, 1573 (2006).
[58] R. L. Anderson, Solid-State Electron. **5**, 341 (1962).
[59] V. E. Henrich and P. A. Cox, *The Surface Science of Metal Oxides* (Cambridge University Press, Cambridge, 1994).